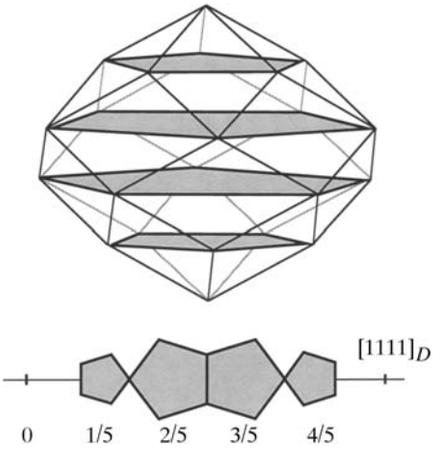

Fig. 4.6.3.15. Atomic surface of the Penrose tiling in the 5D hypercubic description. The projection of the 5D hypercubic unit cell upon $\mathbf{V}^{\perp}$ gives a rhomb-icosahedron (above). The Penrose tiling is generated by four equidistant pentagons (shaded) inscribed in the rhomb-icosahedron. Below is a perpendicular-space projection of the same pentagons, which are located on the $[1111]_D$ diagonal of the 4D hyper-rhombohedral unit cell in the 4D description.

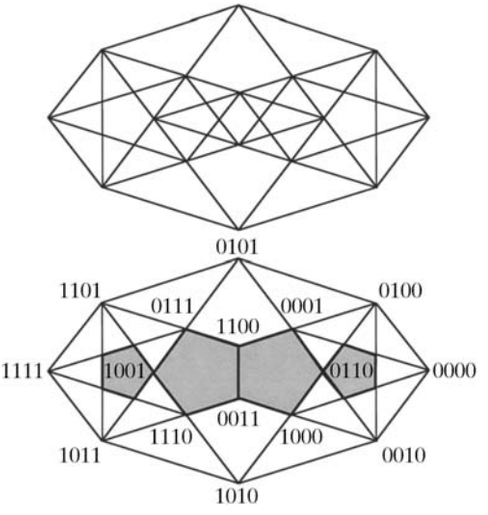

Fig. 4.6.3.16. Projection of the 4D hyper-rhombohedral unit cell of the Penrose tiling in the 4D description upon the perpendicular space. In the upper drawing all edges between the 16 corners are shown. In the lower drawing the corners are indexed and the four pentagonal atomic surfaces of the Penrose tiling are shaded.

$$W = \begin{pmatrix} a_1^* \cos(2\pi/5) & a_2^* \cos(4\pi/5) & a_3^* \cos(6\pi/5) & a_4^* \cos(8\pi/5) \\ a_1^* \sin(2\pi/5) & a_2^* \sin(4\pi/5) & a_3^* \sin(6\pi/5) & a_4^* \sin(8\pi/5) \\ \hline a_1^* \cos(4\pi/5) & a_2^* \cos(8\pi/5) & a_3^* \cos(2\pi/5) & a_4^* \cos(6\pi/5) \\ a_1^* \sin(4\pi/5) & a_2^* \sin(8\pi/5) & a_3^* \sin(2\pi/5) & a_4^* \sin(6\pi/5) \end{pmatrix}.$$

The 2D Penrose tiling can also be embedded canonically in the 5D space. Canonically means that the 5D lattice is hypercubic and that the projection of one unit cell upon the 3D perpendicular space $\mathbf{V}^{\perp}$, giving a rhomb-icosahedron, defines the atomic surface. However, the parallel-space image $\mathbf{a}_i^*$, $i = 1, \ldots, 4$, with $\mathbf{a}_0^* = -(\mathbf{a}_1^* + \mathbf{a}_2^* + \mathbf{a}_3^* + \mathbf{a}_4^*)$, of the 5D basis $\mathbf{d}_i^*$, $i = 1, \ldots, 4$ is not linearly independent. Consequently, the atomic surface consists of only a subset of the points contained in the rhomb-icosahedron: five equidistant pentagons (one with diameter zero) resulting as sections of the rhomb-icosahedron with five equidistant parallel planes (Fig. 4.6.3.15). The linear dependence of the 5D basis allows the embedding in the 4D space. The resulting hyper-rhombohedral hyperlattice is spanned by the basis $\mathbf{d}_i$, $i = 1, \ldots, 4$, discussed above. The atomic surfaces occupy the positions $p/5(1111)$, $p = 1, \ldots, 4$, on the body diagonal of the 4D unit cell. Neighbouring pentagons are in an *anti* position to each other (Fig. 4.6.3.16). Thus the 4D unit cell is decorated centrosymmetrically. The edge length a_r of a Penrose rhomb is related to the length of physical-space basis vectors a_i^* by $a_r = \tau S$, with the smallest distance $S = (2\tau/5a_i^*)$, $i = 1, \ldots, 4$. The *point density* (number of vertices per unit area) of a Penrose tiling with Penrose rhombs of edge length a_r can be calculated from the ratio of the relative number of unit tiles in the tiling to their area:

$$\rho = \frac{1+\tau}{a_r^2[\sin(\pi/5) + \tau \sin(2\pi/5)]} = (5/2)a_i^{*2}(2-\tau)^2 \tan(2\pi/5).$$

This is equivalent to the calculation from the 4D description,

$$\rho = \frac{\sum_{i=1}^{4} \Omega_{\rm AS}^i}{\Omega_{\rm UC}} = \frac{\sum_{i=1}^{4} (5/2)\lambda^2 \sin(2\pi/5)}{4/[5(5)^{1/2}|a_i^*|^4]} = (5/2)a_i^{*2}(2-\tau)^2 \tan(2\pi/5),$$

where $\Omega_{\rm AS}$ and $\Omega_{\rm UC}$ are the area of the atomic surface and the volume of the 4D unit cell, respectively. The pentagon radii are $\lambda_{1,4} = 2(2-\tau)/5a^*$ and $\lambda_{2,3} = 2(\tau-1)/5a^*$ for the atomic surfaces in $(p/5)(1111)$ with $p = 1, 4$ and $p = 2, 3$. A detailed discussion of the properties of Penrose tiling is given in the papers of Penrose (1974, 1979), Jaric (1986) and Pavlovitch & Kleman (1987).

4.6.3.3.2.1. Indexing

The indexing of the submodule M_1^* of the diffraction pattern of a decagonal phase is not unique. Since M_1^* corresponds to a $\mathbb{Z}$ module of rank 4 with decagonal point symmetry, it is invariant under scaling by $\tau^n, n \in \mathbb{Z}$: $S^n M^* = \tau^n M^*$. Nevertheless, an optimum basis (low indices are assigned to strong reflections) can be derived: not the metrics, as for regular periodic crystals, but the intensity distribution characterizes the best choice of indexing.

A correct set of reciprocal-basis vectors can be identified experimentally in the following way:

(1) Find directions of systematic absences or pseudo-absences determining the possible orientations of the reciprocal-basis vectors (see Rabson *et al.*, 1991).

(2) Find pairs of strong reflections whose physical-space diffraction vectors are related to each other by the factor τ.

(3) Index these reflections by assigning an appropriate value to a^*. This value should be derived from the shortest interatomic distance S and the edge length of the unit tiles expected in the structure.

(4) The reciprocal basis is correct if all observable Bragg reflections can be indexed with integer numbers.

4.6.3.3.2.2. Diffraction symmetry

The diffraction symmetry of decagonal phases can be described by the Laue groups $10/mmm$ or $10/m$. The set of all vectors $\mathbf{H}$ forms a Fourier module $M^* = \{\mathbf{H}^{\parallel} = \sum_{i=1}^{5} h_i \mathbf{a}_i^* | h_i \in \mathbb{Z}\}$ of rank 5 in physical space which can be decomposed into two submodules $M^* = M_1^* \oplus M_2^*$. $M_1^* = \{h_1\mathbf{a}_1^* + h_2\mathbf{a}_2^* + h_3\mathbf{a}_3^* + h_4\mathbf{a}_4^*\}$ corresponds to a $\mathbb{Z}$ module of rank 4 in a 2D subspace, $M_2^* = \{h_5\mathbf{a}_5^*\}$ corresponds to a $\mathbb{Z}$ module of rank 1 in a 1D subspace. Consequently, the first submodule can be considered as a projection from a 4D reciprocal lattice, $M_1^* = \pi^{\parallel}(\Sigma^*)$, while the second submodule is of the form of a regular 1D reciprocal lattice, $M_2^* = \Lambda^*$. The diffraction pattern of the Penrose tiling decorated with equal point scatterers on its vertices is shown in Fig. 4.6.3.17. All Bragg reflections within

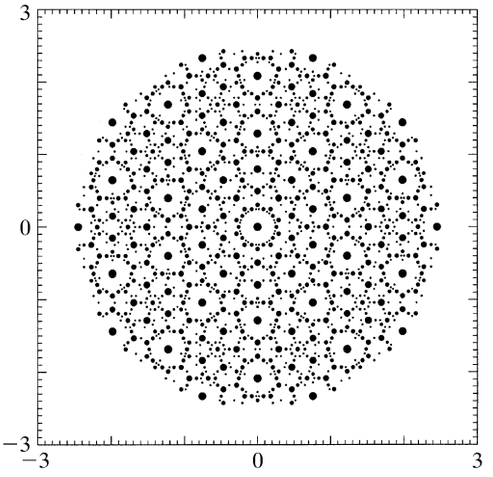

Fig. 4.6.3.17. Schematic diffraction pattern of the Penrose tiling (edge length of the Penrose unit rhombs a_r = 4.04 Å). All reflections are shown within $10^{-2}|F(\mathbf{0})|^2 < |F(\mathbf{H})|^2 < |F(\mathbf{0})|^2$ and $0 \le |\mathbf{H}^{\parallel}| \le 2.5$ Å^{-1}.

$10^{-2}|F(\mathbf{0})|^2 < |F(\mathbf{H})|^2 < |F(\mathbf{0})|^2$ are depicted. Without intensity-truncation limit, the diffraction pattern would be densely filled with discrete Bragg reflections. To illustrate their spatial and intensity distribution, an enlarged section of Fig. 4.6.3.17 is shown in Fig. 4.6.3.18. This picture shows all Bragg reflections within $10^{-4}|F(\mathbf{0})|^2 < |F(\mathbf{H})|^2 < |F(\mathbf{0})|^2$. The projected 4D reciprocal-lattice unit cell is drawn and several reflections are indexed. All reflections are arranged along lines in five symmetry-equivalent orientations. The perpendicular-space diffraction patterns (Figs. 4.6.3.19 and 4.6.3.20) show a characteristic star-like distribution of the Bragg reflections. This is a consequence of the pentagonal shape of the atomic surfaces: the Fourier transform of a pentagon has a star-like distribution of strong Fourier coefficients.

The 5D decagonal space groups that may be of relevance for the description of decagonal phases are listed in Table 4.6.3.1. These space groups are a subset of all 5D decagonal space groups fulfilling the condition that the 5D point groups they are associated with are isomorphous to the 3D point groups describing the diffraction symmetry. Their structures are comparable to 3D hexagonal groups. Hence, only primitive lattices exist. The orientation of the symmetry elements in the 5D space is defined by the isomorphism of the 3D and 5D point groups. However, the action of the tenfold rotation is different in the subspaces $\mathbf{V}^{\parallel}$ and

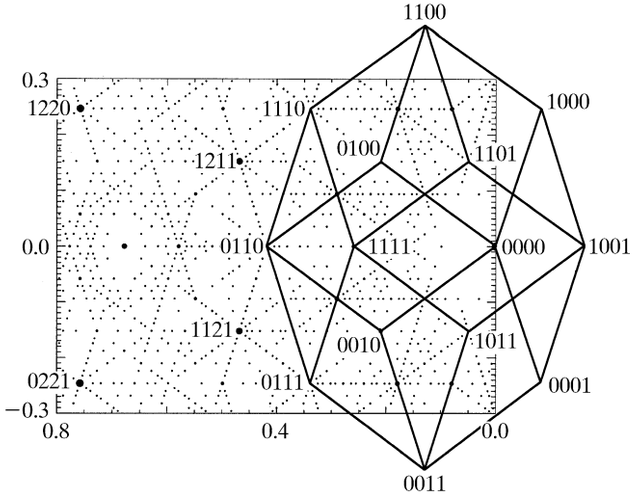

Fig. 4.6.3.18. Enlarged section of Fig. 4.6.3.17. All reflections shown are selected within the given limits from a data set within $10^{-4}|F(\mathbf{0})|^2 < |F(\mathbf{H})|^2 < |F(\mathbf{0})|^2$ and $0 \le |\mathbf{H}^{\parallel}| \le 2.5$ Å^{-1}. The projected 4D reciprocal-lattice unit cell is drawn and several reflections are indexed.

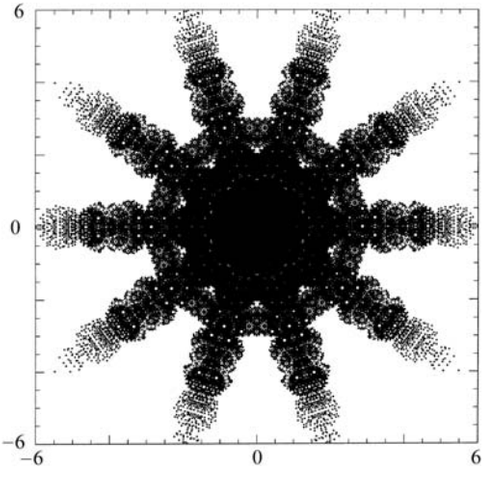

Fig. 4.6.3.19. The perpendicular-space diffraction pattern of the Penrose tiling (edge length of the Penrose unit rhombs a_r = 4.04 Å). All reflections are shown within $10^{-4}|F(\mathbf{0})|^2 < |F(\mathbf{H})|^2 < |F(\mathbf{0})|^2$ and $0 \le |\mathbf{H}^{\parallel}| \le 2.5$ Å^{-1}.

$\mathbf{V}^{\perp}$: a rotation of $\pi/5$ in $\mathbf{V}^{\parallel}$ is correlated with a rotation of $3\pi/5$ in $\mathbf{V}^{\perp}$. The reflection and inversion operations are equivalent in both subspaces.

4.6.3.3.2.3. Structure factor

The structure factor for the decagonal phase corresponds to the Fourier transform of the 5D unit cell,

$$F(\mathbf{H}) = \sum_{k=1}^{N} f_k(\mathbf{H}^{\parallel}) T_k(\mathbf{H}^{\parallel}, \mathbf{H}^{\perp}) g_k(\mathbf{H}^{\perp}) \exp(2\pi i \mathbf{H} \cdot \mathbf{r}_k),$$

with 5D diffraction vectors $\mathbf{H} = \sum_{i=1}^{5} h_i \mathbf{d}_i^*$, N hyperatoms, parallel-space atomic scattering factor $f_k(\mathbf{H}^{\parallel})$, temperature factor $T_k(\mathbf{H}^{\parallel}, \mathbf{H}^{\perp})$ and perpendicular-space geometric form factor $g_k(\mathbf{H}^{\perp})$. $T_k(\mathbf{H}^{\parallel}, \mathbf{0})$ is equivalent to the conventional Debye–Waller factor and $T_k(\mathbf{0}, \mathbf{H}^{\perp})$ describes random fluctuations along the perpendicular-space coordinate. These fluctuations cause characteristic jumps of vertices in physical space (*phason flips*). Even random phason flips map the vertices onto positions which can still be described by physical-space vectors of the type $\mathbf{r} = \sum_{i=1}^{5} n_i \mathbf{a}_i$. Consequently, the set $M = \{\mathbf{r} = \sum_{i=1}^{5} n_i \mathbf{a}_i | n_i \in \mathbb{Z}\}$ of all possible vectors forms a $\mathbb{Z}$ module. The shape of the atomic surfaces corresponds to a selection rule for the positions actually occupied. The geometric form factor $g_k(\mathbf{H}^{\perp})$ is equivalent to the

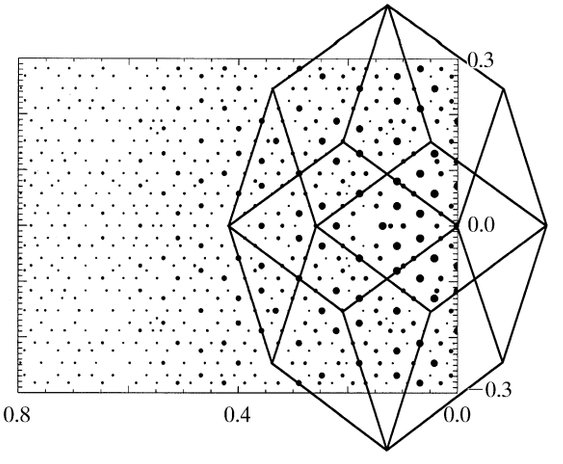

Fig. 4.6.3.20. Enlarged section of Fig. 4.6.3.19 showing the projected 4D reciprocal-lattice unit cell.

references